Gamma-Ray and X-Ray Observations of the Periodic-repeater FRB 180916 during Active Phases

M. Tavani[1,2], F. Verrecchia[3,4], C. Casentini[1,5], M. Perri[3,4], A. Ursi[1], L. Pacciani[1], C. Pittori[3,4], A. Bulgarelli[6], G. Piano[1], M. Pilia[7], G. Bernardi[8,9], A. Addis[6], L. A. Antonelli[4], A. Argan[1], L. Baroncelli[6,10], P. Caraveo[11,12], P. W. Cattaneo[12], A. Chen[13], E. Costa[1], G. Di Persio[1], I. Donnarumma[14], Y. Evangelista[1], M. Feroci[1], A. Ferrari[15], V. Fioretti[6], F. Lazzarotto[16], F. Longo[17], A. Morselli[5], F. Paoletti[1,18], N. Parmiggiani[6,19], A. Trois[7], S. Vercellone[20], G. Naldi[8], G. Pupillo[8], G. Bianchi[8], and S. Puccetti[14]

[1] INAF/IAPS, via del Fosso del Cavaliere 100, I-00133 Roma (RM), Italy; marco.tavani@inaf.it, claudio.casentini@inaf.it
[2] Università degli Studi di Roma Tor Vergata, via della Ricerca Scientifica 1, I-00133 Roma (RM), Italy
[3] SSDC/ASI, via del Politecnico snc, I-00133 Roma (RM), Italy; francesco.verrecchia@inaf.it
[4] INAF/OAR, via Frascati 33, I-00078 Monte Porzio Catone (RM), Italy
[5] INFN Sezione di Roma 2, via della Ricerca Scientifica 1, I-00133 Roma (RM), Italy
[6] INAF/OAS, via Gobetti 101, I-40129 Bologna (BO), Italy
[7] INAF/OACa, via della Scienza 5, I-09047 Selargius (CA), Italy
[8] INAF/IRA, via Piero Gobetti 101, I-40129 Bologna (BO), Italy
[9] Department of Physics and Electronics, Rhodes University, P.O. Box 94, Grahamstown 6140, South Africa
[10] Dip. di Fisica e Astronomia, Università di Bologna, Viale Berti Pichat 6/2, I-40127 Bologna, Italy
[11] INAF/IASF, via E. Bassini 15, I-20133 Milano (MI), Italy
[12] INFN Sezione di Pavia, via U. Bassi 6, I-27100 Pavia (PV), Italy
[13] School of Physics, Wits University, Johannesburg, South Africa
[14] ASI, via del Politecnico snc, I-00133 Roma (RM), Italy
[15] CIFS, c/o Physics Department, University of Turin, via P. Giuria 1, I-10125 Torino, Italy
[16] INAF/OAPd, vicolo Osservatorio 5, I-35122 Padova (PD), Italy
[17] Dipartimento di Fisica, Università di Trieste and INFN, via Valerio 2, I-34127 Trieste (TR), Italy
[18] East Windsor RSD, 25A Leshin Lane, Hightstown, NJ 08520, USA
[19] Università degli Studi di Modena e Reggio Emilia, DIEF—Via Pietro Vivarelli 10, I-41125 Modena, Italy
[20] INAF/OAB, via Emilio Bianchi 46, I-23807 Merate (LC), Italy

Abstract

FRB 180916 is a most intriguing source capable of producing repeating fast radio bursts with a periodic 16.3 day temporal pattern. The source is well positioned in a star-forming region in the outskirts of a nearby galaxy at 150 Mpc distance. In this Letter we report on the X-ray and γ-ray observations of FRB 180916 obtained by AGILE and Swift. We focused especially on the recurrent 5 day time intervals of enhanced radio bursting. In particular, we report on the results obtained in the time intervals 2020 February 3–8, 2020 February 25, 2020 March 5–10, and 2020 March 22–28 during a multiwavelength campaign involving high-energy and radio observations of FRB 180916. We also searched for temporal coincidences at millisecond timescales between the 32 known radio bursts of FRB 180916 and X-ray and MeV events detectable by AGILE. We do not detect any simultaneous event or any extended X-ray and γ-ray emission on timescales of hours/days/weeks. Our cumulative X-ray (0.3–10 keV) flux upper limit of 5×10^{-14} erg cm^{-2} s^{-1} (obtained during 5 day active intervals from several 1–2 ks integrations) translates into an isotropic luminosity upper limit of $L_{X,\mathrm{UL}} \sim 1.5 \times 10^{41}$ erg s^{-1}. Deep γ-ray observations above 100 MeV over a many-year timescale provide an average luminosity upper limit one order of magnitude larger. These results provide the so-far most stringent upper limits on high-energy emission from the FRB 180916 source. Our results constrain the dissipation of magnetic energy from a magnetar-like source of radius R_m, internal magnetic field B_m, and dissipation timescale τ_d to satisfy the relation $R_{m,6}^3 B_{m,16}^2 \tau_{d,8}^{-1} \lesssim 1$, where $R_{m,6}$ is R_m in units of 10^6 cm, $B_{m,16}$ is B_m in units of 10^{16} G, and $\tau_{d,8}$ in units of 10^8 s.

Unified Astronomy Thesaurus concepts: Gamma-ray astronomy (628); X-ray astronomy (1810); Radio bursts (1339); Radio transient sources (2008); Gamma-ray transient sources (1853)

1. Introduction

Fast radio bursts (FRBs) are impulsive outbursts of mysterious origin (typically lasting $\sim$1 ms) detected in the sub-GHz and GHz bands (e.g., Lorimer et al. 2007; Cordes & Chatterjee 2019). Most of the FRBs have been detected only once, but a special category of repeating FRBs has been recently revealed, demonstrating that a subclass of sources can produce multiple radio outbursts over timescales of years (Cordes & Chatterjee 2019; Petroff et al. 2019).

We focus here on the remarkable repeater FRB 180916. J0158+65 (hereafter FRB 180916) for which 35 radio bursts

have been detected with a periodic pattern during the time interval 2018 September–2019 October (CHIME/FRB Collaboration et al. 2020, hereafter C20). This source, originally localized by CHIME/FRB with an uncertainty of about 0.09 deg^2 (CHIME/FRB Collaboration et al. 2019, hereafter C19), was later detected by very long baseline interferometry observations with a precise arcsec positioning (Marcote et al. 2020, hereafter M20). The source is positionally coincident with the outskirts of a spiral galaxy at the distance of about 150 Mpc. The 3σ significance of the proximity of FRB 180916 with a galaxy at a redshift $z = 0.0337 \pm 0.0002$ and

the a posteriori determination of the intergalactic contribution to its observed excess dispersion measure (DM) strongly support the association of FRB 180916 with the galaxy SDSS J015800.28+654253.0 as reported in M20. This repeating FRB source is therefore located at a distance significantly smaller than that of the majority of FRBs showing $DM_{excess} \geqslant 100 \, pc \, cm^{-3}$ where DM_{excess} is the excess DM once the Galactic and halo contributions are taken into account.

Evidence of periodic activity of radio bursting from FRB 180916 provides important clues on the mechanism of FRB generation from this source (C20). Radio bursts are not randomly distributed but appear to concentrate especially in specific 5 day intervals recurring every 16.35 days. As noted in C20, this period can be affected by aliasing[21] due to the CHIME/FRB regular exposure pattern of FRB 180916. A periodic behavior of an otherwise unpredictable emission is remarkable, and suggests either a "triggering" of the radio bursting from physical interactions in a binary system, or emission influenced by compact star precession.

FRB 180916 is then worth a careful study, given its relevance in terms of proximity, number of detected radio bursts, and periodic activity. Table 1 summarizes the relevant information on the 32 radio bursts so far detected from FRB 180916, providing topocentric arrival times and radio fluences on millisecond timescales. The (isotropic-equivalent) energy involved in the radio burst emissions is in the range $E_{radio,iso} \simeq (10^{36}–10^{38} \, erg)$ at the source distance, which is a value million times larger than that of the brightest giant pulses observed from the Crab pulsar (Hankins et al. 2003). The object underlying FRB 180916 is therefore exceptional in its emission properties.

We recently presented in Casentini et al. (2020) preliminary results of AGILE observations of FRB 180916 based on the first 10 detected radio bursts. In this Letter we extend our search for high-energy emission from the source considering Swift X-ray observations as well as AGILE γ-ray data both focused on specific active 5 day repetition intervals. Our observations are part of a multifrequency campaign involving AGILE, Swift, and radio observations of FRB 180916 during the periods 2020 February 3–8 and 2020 February 19–25 carried out at the Sardinia Radio Telescope (Prandoni et al. 2017) and at the Northern Cross in Medicina (Locatelli et al. 2020). Our improved upper limits on X-ray and γ-ray emissions from FRB 180916 provide significant constraints on the physical nature of FRB 180916.

2. AGILE Observations

The AGILE mission is an Italian Space Agency (ASI) space project dedicated to X-ray and γ-ray astrophysics (Tavani et al. 2009; Tavani 2019). The instrument consists of four different detectors on board the satellite: an imaging γ–ray Silicon Tracker sensitive in the range 30 MeV–30 GeV (GRID; Barbiellini et al. 2002), a coded mask X-ray imager sensitive in the 18–60 keV band (Super-AGILE; Feroci et al. 2007), the Mini-Calorimeter sensitive in the 0.4–100 MeV band (MCAL; Labanti et al. 2009), and the anticoincidence (Perotti et al. 2006) system. Currently, AGILE operates in spinning mode (Pittori 2019), with the instrument axis rotating every ∼7

minutes around the satellite–Sun direction; for each satellite revolution, an exposure of about 80% of the entire sky is obtained. For a summary of the AGILE mission features, see Tavani (2019).

AGILE is capable of quasi-continuously monitoring a source positioned in the accessible portion of the sky. Source visibility depends on solar panel constraints (a seasonal effect that makes about 20% of the sky near the Sun or in the opposite direction not available for observations at any given time), Earth occultations (affecting source visibility with ∼10^{3} s time-scales), and the South Atlantic Anomaly (affecting about 10% of the ∼95 minute satellite orbit). Despite these limitations, AGILE can be very effective in detecting transient and steady X-ray and γ-ray emissions from cosmic sources.

In this Letter we focus on AGILE and Swift observations of the FRB 180916 location (Galactic coordinates $l = 129°.7$, $b = 3°.7$) that turns out to be somewhat influenced by diffuse Galactic emission. The results of the analysis of radio observations (Pilia et al. 2020a) will be reported in a separated paper (Pilia et al. 2020b). In the following we report the results of searches for high-energy emission in coincidence with the arrival times (T_0) of Table 1 within time windows of 200 s centered at T_0. Due to dispersive delay, radio waves reach detectors on Earth or in orbit several seconds after X-rays or γ-rays. In our searches we take as T_0 the de-dispersed topocentric arrival times[22] at infinite frequencies for the different radio telescopes of Table 1.

2.1. Super-A Flux Upper Limits

Super-AGILE detects steady and transient emission from sources in the 18–60 keV energy band within a field of view of $107° \times 68°$. Due to the spinning of the AGILE satellite, we analyzed time periods with the source within $10°$ from the instrument on-axis direction. The resulting time windows have a duration of about 10–20 s. We excluded events taken during the passage above the South Atlantic Anomaly, and events collected when the source was occulted by the Earth. We searched for hard X-ray emission during the 5 day active periods of FRB 180916 during the intervals 2020 February 3–8 and 2020 February 19–25. The corresponding effective exposures of 5.6 and 2.4 ks lead to 5σ ULs of 2.4 and $5.0 \times 10^{-9} \, erg \, cm^{-2} \, s^{-1}$ for the two observing intervals. For the sum of observations during the interval 2020 February 3–25, we obtain an upper limit of $1.8 \times 10^{-9} \, erg \, cm^{-2} \, s^{-1}$ for a total exposure of 13.5 ks.

2.2. MCAL Fluence Upper Limits

The AGILE/MCAL (Marisaldi et al. 2008; Labanti et al. 2009) is an all-sky monitor with a 4π field of view (FoV), sensitive in the 400 keV–100 MeV energy range. It is a segmented detector, composed of 30 CsI(Tl) scintillation bars, with a total geometrical area of ∼1400 cm^2 (on-axis). The AGILE MCAL is a triggered detector: its onboard trigger logic acts on different energy ranges and timescales (ranging from ∼300 μs to ∼8 s). The submillisecond logic timescale allows MCAL to trigger on very short-duration impulsive events. MCAL is then capable of efficiently detecting long and short transients such as GRBs (Galli et al. 2013) as well as terrestrial

---

[21] The resulting period could be in the range of a few hours to a day as discussed in C20. However, C20 discuss several possibilities that support the hypothesis that this is not the case.

[22] The difference between the actual AGILE arrival time and the radio telescopes' de-dispersed topocentric times is of order of 20–40 ms, and it is negligible for our adopted window search of 200 s.

Table 1
FRB180916.J0158+65 Bursts and AGILE Observations

		FRB Parameters				Event in the AGILE FoV		
Burst No.	Date	Arrival Times[a] (UTC)	Instr.[b]	Bandwidth (MHz)	Fluence (Jy ms)	MCAL	GRID	Super-A
1	2018 Sep 16	10:15:10.746748	C	400–800	>2.3	NO	NO	NO
2	2018 Oct 19	08:13:13.695545	C	400–800	>3.5	⋯	⋯	⋯
3	2018 Oct 19	08:13:13.759080	C	400–800	>2.0	⋯	⋯	⋯
4	2018 Nov 4	06:57:09.522136	C	400–800	>2.8	YES	NO	NO
5	2018 Nov 4	07:06:52.655909	C	400–800	6.8	YES	NO	NO
6	2018 Nov 20	05:55:57.158955	C	400–800	8.0	YES	NO	NO
7	2018 Dec 22	03:59:14.238510	C	400–800	9.6/15/16.5/7.2	YES	YES	NO
8	2018 Dec 23	03:51:19.892113	C	400–800	10.4/3.6	YES	YES	NO
9	2018 Dec 25	03:52:54.884107	C	400–800	3.1	YES	NO	NO
10	2018 Dec 26	03:43:21.063337	C	400–800	2.9/1.6	YES	NO	NO
11	2019 Jan 26	01:32:41.297440	C	400–800	6.4	⋯	⋯	⋯
12	2019 May 18	18:13:33.601287	C	400–800	1.0	⋯	⋯	⋯
13	2019 May 18	18:20:56.937173	C	400–800	7.7	NO	NO	NO
14	2019 May 19	17:50:16.601726	C	400–800	>1.3/>2.2	YES	YES	NO
15	2019 May 19	18:08:52.454119	C	400–800	3.1/5.3	⋯	⋯	⋯
16	2019 May 19	18:10:41.139009	C	400–800	4.4	NO	NO	NO
17	2019 Jun 3	17:09:14.367599	C	400–800	2.1	YES	NO	NO
18	2019 Jun 4	17:11:30.757683	C	400–800	37	⋯	⋯	⋯
19	2019 Jun 5	16:55:55.866635	C	400–800	>7.0	NO	NO	NO
20	2019 Jun 5	17:02:21.845335	C	400–800	11.5/5.4	NO	NO	NO
21	2019 Jun 19	02:24:19.980000	E	1636–1764	0.72	YES	NO	NO
22	2019 Jun 19	02:46:06.367000	E	1636–1764	0.20	YES	YES	NO
23	2019 Jun 19	03:36:59.608000	E	1636–1764	0.62	⋯	⋯	⋯
24	2019 Jun 19	06:46:56.344000	E	1636–1764	2.53	YES	NO	NO
25	2019 Aug 9	12:50:40.150674	C	400–800	7.3	YES	NO	NO
26	2019 Aug 10	12:49:34.408294	C	400–800	>1.7	⋯	⋯	⋯
27	2019 Aug 25	11:48:18.617542	C	400–800	24	NO	NO	NO
28	2019 Aug 25	11:51:53.904598	C	400–800	2.8	NO	NO	NO
29	2019 Aug 25	11:51:53.967298	C	400–800	1.4	NO	NO	NO
30	2019 Aug 25	11:53:35.794063	C	400–800	>2.6	NO	NO	NO
31	2019 Oct 30	07:33:47.920217	C	400–800	2.3	⋯	⋯	⋯
32	2019 Oct 30	07:41:43.668377	C	400–800	>2.3	YES	YES	YES
33	2020 Feb 20	13:27:35.57	S	296–360	37	YES	YES	⋯
34	2020 Feb 20	13:36:49.57	S	296–360	13	⋯	⋯	⋯
35	2020 Feb 20	13:36:49.57	S	296–360	19	⋯	⋯	⋯

Notes. Unmarked detector FoV labels are for radio events occurring when the AGILE instrument was in idle mode with no data acquisition mostly due to passages over the SAA.
[a] De-dispersed topocentric arrival times at the CHIME, Effelsberg, or SRT locations.
[b] Radio instruments that detected each specific burst, where C is for CHIME/FRB, E for EVN, and S for SRT.

Table 2
Average AGILE/MCAL Fluence ULs in erg cm^{-2}

Sub-ms	1 ms	16 ms	64 ms	256 ms	1024 ms	8192 ms
1.13×10^{-8}	1.29×10^{-8}	3.72×10^{-8}	4.97×10^{-8}	7.95×10^{-8}	1.59×10^{-7}	4.49×10^{-7}

gamma-ray flashes on millisecond timescales (Marisaldi et al. 2015). A detailed discussion about MCAL triggering and upper limit capabilities is reported in Casentini et al. (2020) and Ursi et al. (2019).

We checked the possible detections by MCAL of transient emission at or near the times of arrival of all accessible radio burst events marked with a "YES" label in the MCAL column of Table 2. Our search was within ±100 s from the topocentric arrival times of Table 1. An example of the AGILE satellite pointing near the arrival time of event n. 32 of Table 1 is given in Figure 1.

No significant event was detected for a typical fluence UL obtained for millisecond timescales of 10^{-8} erg cm^{-2}. Table 2 provides the typical MCAL fluence ULs obtained at different trigger timescales. When compared with the radio fluences of FRB 180916 bursts, our ULs in the MeV range set the constraint that the energy detectable in the MeV range and emitted on millisecond timescales have to be less than $\sim 10^8$ times the energy emitted in the GHz band ($E_r \sim 3 \times 10^{37}$ erg).

2.3. GRID Flux Upper Limits

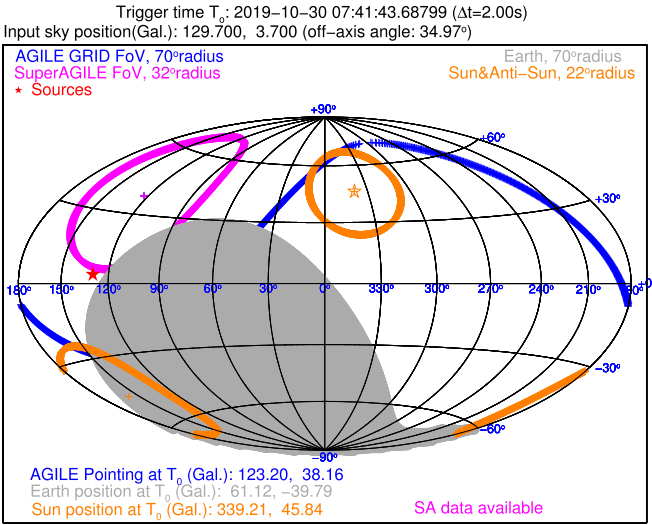Gamma-ray observations of FRB 180916 focused on day-long exposures of the source during the reportedly active time

Figure 1. Galactic coordinate map showing the AGILE/GRID FoV (in blue color) and the Super-A FoV (in magenta color) at the time of arrival T_0 of the FRB 180916 radio burst No. 32 of Table 1 on 2019 October 30 07:41:43.668 UTC. The position of FRB 180916 is marked with a red star. The shaded gray area shows the portion of the sky occulted by the Earth at T_0.

intervals following the 16.3 periodicity of C20. Table 3 summarizes the AGILE/GRID ULs obtained above 100 MeV for 5 day integrations corresponding to 10 contiguous active intervals of FRB 180916 covering the period 2019 August 23 (see Table 4). Typical 5 day GRID flux ULs are $10^{-10}\,\mathrm{erg\,cm^{-2}\,s^{-1}}$ (obtained by the AGILE multisource maximum likelihood analysis for a power-law spectral model of spectral photon index of 2) corresponding to isotropic-equivalent γ-ray luminosity ULs of $3 \times 10^{44}\,\mathrm{erg\,s^{-1}}$.

In addition to the latter integrations, we also performed a deep exposure of the FRB 180916 region including both pointing (2007–2009) and spinning (2010–today) mode data. We find an integrated flux UL $\sim 8.2 \times 10^{-13}\,\mathrm{erg\,cm^{-2}\,s^{-1}}$, corresponding to an isotropic long-term averaged γ-ray luminosity $L_{\gamma,\mathrm{UL,ave}} \sim 2 \times 10^{42}\,\mathrm{erg\,s^{-1}}$.

3. Swift Observations

The Neil Gehrels Swift Gamma-ray Burst Observatory has three instruments (Gehrels et al. 2004), namely, the Burst Alert Telescope (Markwardt et al. 2005), the X-ray Telescope (XRT; Burrows et al. 2005), and the Ultraviolet/Optical Telescope. A request for Swift Target of Opportunity (ToO) observations of FRB 180916 was granted, and a first 6 day period of pointings started on 2020 February 3. An additional observation on 2020 February 25 was also carried out (solar panel constraints did not allow Swift to monitor the corresponding active time interval). Additional Swift data were collected during the active time intervals 2020 March 5–10 and 2020 March 22–28.

3.1. Swift/XRT Flux Upper Limits

The XRT data were taken within the framework of the planned coordinate multi-instrument campaign. The FRB 180916 position was monitored in the X-rays (0.3–10 keV) during a first interval with daily observations between MJD 58882 and MJD 58887 (Tavani et al. 2020a, 2020b). A single observation was carried out on MJD 58904. Additional pointings were obtained during the time windows MJD 58913–58918 and MJD 58921–58926. All observations were

carried out in the Photon Counting readout mode, with a typical exposure of $\sim$1.5 ks per pointing. The data were processed using the XRTDAS software package (v.3.5.0), developed by the ASI Space Science Data Center (SSDC) and released by HEASARC in the HEASoft package (v.6.26.1). The data were calibrated and cleaned with standard filtering criteria using the xrtpipeline task and the calibration files available from the Swift/XRT CALDB (version 20190910). The imaging analysis was executed selecting events in the energy channels between 0.3 and 10 keV and within a 10 pixel ($\sim$46″) radius, which contains 80% of the point-spread function. The background was estimated from an annular region with radii of 25 and 60 pixels. No X-ray source was detected. We extracted the 3σ countrates UL using the XIMAGE package (*sosta* command) and converted to fluxes using a standard single power-law spectral model with photon index $\alpha = 2.0$ (with the photon number flux defined as $dN/d\varepsilon \propto \varepsilon^{-\alpha}$, with ε the photon energy). We corrected the flux for absorption with a neutral-hydrogen (N_H) column density fixed to the Galactic 21 cm value in the direction of the source, $7.1 \times 10^{21}\,\mathrm{cm^{-2}}$ (HI4PI Collaboration et al. 2016), and redshifted the single spectral component for the known value $z = 0.0337$ (M20).[23] Combining all the Swift/XRT observations we obtain an overall 3σ flux upper limit of $3.1 \times 10^{-14}\,\mathrm{erg\,cm^{-2}\,s^{-1}}$ for the total exposures of 26.8 ks. The X-ray ULs are reported in Table 5. Figure 2 shows a summary of AGILE-GRID and Swift observations.

4. Discussion

Our X-ray and γ-ray observations of FRB 180916 provide valuable constraints on the nature of the source. The (isotropic-equivalent) energy of radio bursts is $E_{\mathrm{radio,iso}} \simeq (3 \times 10^{37}\,\mathrm{erg})$ $S_{\nu,\mathrm{Jy}}\ \delta t_{\mathrm{ms}}\ \Delta\nu_{\mathrm{GHz}}\ d_{150M}^2$, where the measured radio flux density is $S_{\nu,\mathrm{Jy}}$ in units of Jansky, δt_{ms} is the temporal width in units of milliseconds, $\Delta\nu_{\mathrm{GHz}}$ is the radio bandwidth in units of GHz, and $d_{150\mathrm{Mpc}} = d/150\,\mathrm{Mpc}$ with d the source distance from Earth. Note from Table 1 that the radio bursts of FRB 180916 have radio spectral fluences F'_{GHz} in the range $0.1\,\mathrm{Jy\,ms} \lesssim F'_{\mathrm{GHz}} \lesssim 10\,\mathrm{Jy\,ms}$ for frequencies in the interval 0.3–1.5 GHz. We therefore have $E_{\mathrm{radio,iso}} \simeq (10^{36}$–$10^{38})$ erg that is radiated on millisecond timescales. These energies are 6 orders of magnitude larger than those of the giant pulses from the Crab pulsar (Hankins et al. 2003). It is therefore unlikely that the underlying source of FRB 180916 is a neutron star of the type associated with radio pulsars in our Galaxy. Alternative possibilities to provide the required energies rely on compact objects, either strongly magnetized objects such as magnetars, or black holes (BHs). In both cases, the energetics involved in the impulsive radio emission might be a small fraction of a much larger latent power. The process of radio burst emission in FRB 180916 is probably "triggered" by the presence of a companion star. We can envision different possibilities for the generation of radio pulses induced by a wind or plasma flow originating from a companion (main sequence, O–B, or Be) star: magnetospheric events, accretion events, or shock interactions with mass outflows under the form of isotropic or equatorial winds as in the case of Be stars. Alternative scenarios include periodicities induced by a

---

[23] We verified that variations in photon index of ± 0.5 lead to flux values within $-20\%/+30\%$ with respect to the one reported above; variations of N_H from 10^{21} to $10^{22}\,\mathrm{cm^{-2}}$ correspond to variations in flux values within $\lesssim 30\%$.

Table 3
Average AGILE/GRID Flux ULs in erg cm^{-2} s^{-1}

$\Delta T = 10^1$ s	$\Delta T = 10^2$ s	$\Delta T = 10^3$ s	$\Delta T = 10^0$ days	$\Delta T = 10^1$ days	$\Delta T = 10^2$ days
4.0×10^{-7}	3.5×10^{-8}	1.5×10^{-8}	4.0×10^{-10}	1.0×10^{-10}	**1.7×10^{-11}**

Note. 2σ flux ULs (erg cm^{-2} s^{-1}) obtained for emission in the range 50 MeV–10 GeV for the short integration timescales and 100 MeV–10 GeV for the long ones, at the FRB 180916 position.

Table 4
AGILE/GRID Flux Upper Limits on 5 day Integrations Centered on Single Activity Cycles

Cycle No.	Date[a] (UTC)	UL Value ($\times 10^{-10}$ erg cm^{-2} s^{-1})
3	2020 Mar 25 09:00	2.06
2	2020 Mar 9 00:36	1.42
1	2020 Feb 21 16:12	1.36
0	2020 Feb 5 07:48	0.90
−1	2020 Jan 19 23:24	2.30
−2	2020 Jan 3 15:00	0.74
−3	2019 Dec 18 06:36	0.89
−4	2019 Dec 1 22:12	1.00
−5	2019 Nov 15 13:48	2.10
−6	2019 Oct 30 05:24	1.20
−7	2019 Oct 13 21:00	1.00
−8	2019 Sep 27 12:36	0.76
−9	2019 Sep 11 04:12	1.50
−10	2019 Aug 25 19:48	1.10

Notes. Flux integrations are centered on radio burst activity cycles derived from C20.
[a] Dates refer to the centers of the 5 day time intervals.

Table 5
Swift/XRT 3σ Flux ULs

Start Date (UTC)	Effect. Exposure (s)	0.3–10 keV UL Value ($\times 10^{-13}$ erg cm^{-2} s^{-1})
2020 Feb 3 18:43:55	1677	3.3
2020 Feb 4 15:43:59	1966	2.4
2020 Feb 5 15:23:58	1304	3.5
2020 Feb 6 15:29:51	2006	2.3
2020 Feb 7 15:23:35	2016	2.7
2020 Feb 8 15:16:35	1264	3.4
2020 Feb 25 14:00:01	920	5.4
2020 Mar 5 13:08:00	1828	3.4
2020 Mar 6 14:23:00	1241	3.9
2020 Mar 7 14:16:00	1392	3.3
2020 Mar 8 14:12:13	303	15.0
2020 Mar 9 14:04:46	1597	2.9
2020 Mar 10 13:57:52	920	5.4
2020 Mar 23 12:20:41	1795	3.5
2020 Mar 24 12:40:46	727	7.2
2020 Mar 25 12:40:34	318	18.0
2020 Mar 26 12:20:14	1938	2.3
2020 Mar 27 11:53:55	1738	2.8
2020 Mar 28 11:48:08	1254	3.7

Figure 2. Top panel: (top) AGILE/GRID 5 day γ-ray flux ULs (100 MeV–10 GeV) obtained at active cycles of FRB 180916 during the period 2019 August–2020 March. (bottom) Swift/XRT flux ULs marked in blue color (shown for integrations larger than 900 s) in the 0.3–10 keV energy range; they are obtained for individual observations during cycles 0, 2, and 3 of Table 5 (2020 February 3–8, 2020 February 25, 2020 March 5–10, and 2020 March 23–28). The lowest values of the ULs are for the summed observations of cycle 0 (10.2 ks), cycle 2 (7.9 ks) and cycle 3 (7.8 ks). Bottom panel: AGILE and Swift flux ULs obtained with different integration time intervals of observations of FRB 180916. The GRID ULs (in black color) in the range 50 MeV–10 GeV are for integrations of 10, 100, and 1000 s centered on radio bursts of FRB 180916, and in the range 100 MeV–10 GeV for integrations of 1, 2, and 100 days. The lowest value UL is obtained for a deep GRID integration of ~11.5 yr. Swift/XRT ULs in the 0.3–10 keV energy range (in blue color) are shown for typical single 1.5 ks integrations, summed integration during an active cycle (cycle 0), and for the sum of all observations during cycles 0–3 with a total exposure of 26.8 ks.

compact star precession or localized "spots" in accretion disks. In case of an aliased period shorter than the 16.35 day value, precession or spin of a magnetar-like object should be considered in addition to the binary hypothesis.

We notice that no super-intense radio pulses of the type of FRB 180916 have been detected from binary systems in our Galaxy. Probably t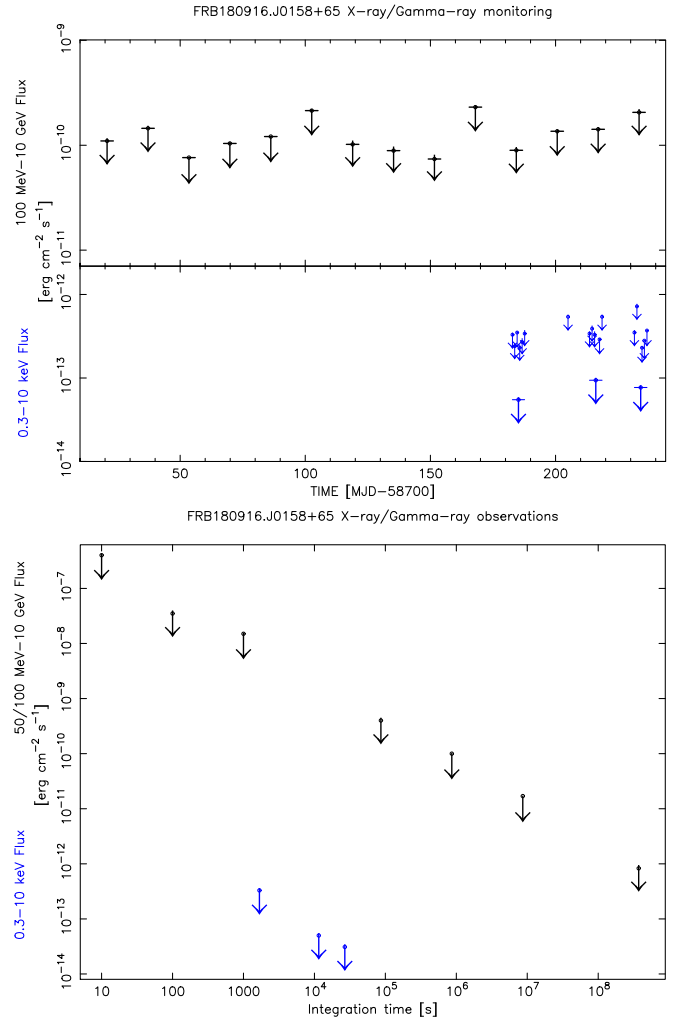he Galactic compact objects that might generate intense radio pulses do not have the right conditions to be "triggered" or induced in a proper way. For example, Galactic magnetar-like objects might miss the right

combination of magnetic field energy and external "trigger" to be effective as FRB sources. Furthermore, no accreting BH in the Galaxy has ever been detected producing short millisecond radio bursts such as those of FRBs. Again, this might be the consequence of external conditions not easily applicable to Galactic systems. We are therefore dealing with an "exotic source" capable of transcending the properties of known compact objects and their environments, either Galactic neutron stars or BHs. Note, however, that rare Galactic radio bursts generated by FRB-like sources might escape detection in searches by multiple-beam receivers as noticeably pointed out by Tendulkar et al. (2016). In this case, the radio flux might be so intense as to saturate momentarily a receiver and be classified as radio frequency interference. It is an interesting possibility for future searches to associate high-energy outbursts with simultaneous (within the delay times) very intense radio events classified as interference.

Before speculating on the nature of the ultimate origin of FRB 180916, it is useful to discuss the energetics. At this moment, we obtained upper limits to the high-energy emission in four different energy bands from X-rays to γ-rays and for different time intervals and integrations. We focus in this Letter on observations during the 5 day FRB-active intervals.

X-ray flux upper limits in the energy range 1–10 keV (for typical integrations of 10^3 s) as obtained by Swift observations. The typical 1–2 ks UL is $F_{X,\mathrm{UL}} \sim 3 \times 10^{-13}$ erg cm^{-2} s^{-1}, corresponding to an isotropic-equivalent X-ray luminosity $L_{X,\mathrm{UL}} \sim 8 \times 10^{41}$ erg s^{-1}. Summing the seven Swift observations of Table 5 we find an integrated UL $F_{X,\mathrm{UL}} \sim 5 \times 10^{-14}$ erg cm^{-2} s^{-1}, corresponding to an isotropic X-ray luminosity $L_{X,\mathrm{UL}} \sim 1.5 \times 10^{41}$ erg s^{-1}.

Hard X-ray upper limits in the range 18–60 keV were obtained by Super-AGILE during periods of favorable exposure in the time interval of this campaign. Summing up the observations, the UL is 1.8×10^{-9} erg cm^{-2} s^{-1}.

MeV fluence upper limits in the range 0.4–1 MeV (at the millisecond level up to seconds) obtained by AGILE/MCAL simultaneous with the FRBs of Table 1 marked with "YES" in the MCAL column. Typical fluence UL in the submillisecond and millisecond ranges of integrations are $F_{\mathrm{MeV,UL}} \sim 10^{-8}$ erg cm^{-2} corresponding to an isotropic MeV energy UL $E_{\mathrm{MeV,UL}} \sim 2 \times 10^{46}$ erg.

GeV flux upper limits in the range 100 MeV–10 GeV (for integrations of hours/days/months) obtained by the AGILE/GRID during active intervals of FRB 180916. The typical 5 day flux UL is $F_{\gamma,\mathrm{UL}} \sim 10^{-10}$ erg cm^{-2} s^{-1}, corresponding to an isotropic-equivalent γ-ray luminosity $L_{\gamma,\mathrm{UL}} \sim 3 \times 10^{44}$ erg s^{-1}. A more stringent limit is obtained by summing all GRID exposures of the FRB 180916 field over the interval 2007–2019: we find an integrated flux UL $F_{\gamma,\mathrm{UL,ave}} \sim 8 \times 10^{-13}$ erg cm^{-2} s^{-1}, corresponding to an isotropic long-term averaged γ-ray luminosity $L_{\gamma,\mathrm{UL,ave}} \sim 2 \times 10^{42}$ erg s^{-1}.

4.1. The Magnetized Neutron Star Hypothesis

Neutron stars of the magnetar-type are natural candidates for a class of FRBs and should be considered for FRB 180916 (for a recent review on magnetars, see Kaspi & Beloborodov 2017). Magnetic instabilities or sudden magnetospheric particle acceleration phenomena can lead to short radio bursts. The action by an "external driver" in a binary system can provide intruding particles and/or electromagnetic fields that may lead to instabilities. The magnetic fields associated with magnetars (of the order of $B_m \sim 10^{14}$–10^{16} G) lead to maximal energies $E_m \sim R_m^3 B_m^2/6 \simeq (2 \times 10^{49} \, \mathrm{erg}) \, R_{m,6}^3 \, B_{m,16}^2$, with $B_{m,16}$ the magnetar inner magnetic field in units of 10^{16} G and where we assumed a magnetospheric radius of the magnetar $R_{m,6} = R_m/(10^6 \, \mathrm{cm})$. A fraction of the total magnetic energy can therefore be dissipated by instabilities on timescales related to plasma relaxation. The ambipolar diffusion (dissipation) timescale of the inner magnetar field has been estimated to be $\tau_d \sim 10^{11}$ s (Thompson & Duncan 1996) and leads to an average dissipated luminosity

$$L_m \sim E_m/\tau_d \sim (10^{38} \, \mathrm{erg \, s^{-1}}) \, R_{m,6}^3 \, B_{m,16}^2 \, \tau_{d,11}^{-1}, \quad (1)$$

where $\tau_{d,11}$ is the dissipation time in units of 10^{11} s. Larger/smaller values of τ_d^{-1} (e.g., Beloborodov 2017) and/or of $B_{m,16}^2$ imply larger/smaller average luminosities. The luminosity L_m of Equation (1) provides a reference value for interpreting our X-ray and γ-ray observations of FRB 180916.

We see that if an instability mechanism is occasionally triggered in the magnetar system, in order to be detected in our observations we require that the object emits within a millisecond in the radio band an energy 10–1000 times larger that that deduced by the average luminosity L_m. This is a demanding but not impossible requirement for a highly magnetized system subject to sudden relaxation (e.g., the case of the soft γ-ray repeater SGR 1806-20; Palmer et al. 2005).

FRB 180916 then might be a magnetar occasionally subject to sudden instabilities that dissipate in a millisecond what normally would have been emitted on longer timescales of order of seconds/minutes/hours. Equation (1) provides a reference luminosity for optical/X-ray/γ-ray emission that should dissipate most of the instability energy. The expected average high-energy flux at the FRB 180916 distance is expected to be

$$F \simeq 4 \quad \times \quad 10^{-17} \, \xi \, b^{-1} \, R_{m,6}^3 \, B_{m,16}^2 \, \tau_{d,11}^{-1} \, \mathrm{erg \, cm^{-2} \, s^{-1}}, \quad (2)$$

where ξ is the conversion factor from magnetic to radiated energies, and b a beaming factor. In order to be detectable in the optical/X-ray/γ-ray band we need enhancements with respect to the average dissipated luminosity L_m by factors of 10^3–10^4. This requirement is certainly demanding, but not impossible to satisfy in a highly unstable system.

Our upper limits therefore constrain the high-energy dissipation related to the active periods of FRB 180916. These considerations based on isotropic emission can be modified to account for beaming effects. If beaming plays a role in the FRB phenomenon, our energy constraints can be made even lower, and approach hour/day luminosities of the order of those of Equation (1).

We conclude that a magnetar with extreme properties in terms of its magnetic field or dissipation process might power the FRB 180916 radio bursts and be detectable in the X-ray range by current instruments.

4.2. The BH Hypothesis

A BH interacting with a gaseous/plasma environment in a binary system should be considered and cannot be discarded based on our data. In order to power the required detectable luminosities the mass of the BH has to be in the range from above solar to hundreds or more of solar masses. The radio and high-energy luminosities to be produced by the BH is most

likely accretion-powered and values larger that that of Equation (1) can be obtained for limited time intervals.

Following Marcote et al. (2020), we remark that the radio position of FRB 180916 is positionally coincident with a remarkable "cusp" of star formation in its host galaxy. If this is not a coincidence, the apparent cusp can actually be a "wake" of stars caused by the presence of a BH of a mass sufficiently large to influence an otherwise ordered flow. Therefore, in principle the BH mass can be of the order of thousands solar masses or more for the presence of an intermediate-mass BH or the remnant of a galactic nucleus as a consequence of a galaxy merging.

The BH hypothesis cannot at the moment be discarded, especially if we consider the energetics of the bulk of FRBs that require energies and luminosities emitted in the radio (and presumably at higher energies) substantially larger than those of FRB 180916 (e.g., Cordes & Chatterjee 2019).

5. Conclusions

AGILE and Swift joint observations of FRB 180916 set important constraints on the energetics of the source by providing the best upper limits on the X-ray and γ-ray emissions.

We focused in this Letter on the 5 day time intervals during which FRB 180916 is more active in producing radio bursts according to C20. A multifrequency campaign of FRB 180916 involved radio (SRT, Northern Cross), X-ray (Swift), and γ-ray (AGILE) observations starting on 2020 February 3 and ending on 2020 February 8. In addition, we retrieved and studied AGILE data for several source active cycles during the time interval 2019 August 25–2020 March 28. We also checked all 35 known radio bursts from FRB 180916 searching for any quasi-simultaneous transient detected by AGILE.

Our best upper limits can be used in the context of a magnetar-like object dissipating its magnetic energy in a timescale τ_d. If B_m is the equivalent strength of the magnetic field that corresponds to the dissipated portion of the magnetic energy, our constraints translate into the relation (assuming $\xi b^{-1} \sim 1$)

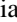$$R_{m,6}^3 \, B_{m,16}^2 \, \tau_{d,8}^{-1} \lesssim 1, \qquad (3)$$
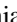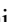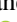
where $\tau_{d,8}$ is in units of 10^8 s. Equation (3) shows that magnetic dissipation (relaxation) timescales of the order of our X-ray and γ-ray observations (10^3–10^5 s) are incompatible with the presence of a very strong magnetic field of the order of 10^{16} G. On the other hand, the very impulsive nature of the FRB phenomenon implying millisecond timescales is indicative of short durations for particle energization and radio emission. Our MeV upper limits obtained at millisecond timescales interpreted in terms of isotropic emission are close to the peak energy detected in the MeV range from SGR 1806-20 (2×10^{46} erg emitted in about 200 ms). After an impulsive phase leading to the radio bursts, the system may "relax" on a longer timescale with associated X-ray and possibly γ-ray emission. Equation (3) is then an important (and best so far) constraint in the context of a magnetar model for FRB 180916.

The search for high-energy counterparts of FRB sources continues, and more data on FRB 180916 and other FRBs are necessary. Considering the variability in the interaction between a companion star and a compact object near periastron as observed in X-ray binaries, a systematic monitoring of FRB 180916 is necessary. AGILE will then continue to monitor and search for high-energy emissions from FRB 180916, our so-far unique periodic-repeating FRB.

ORCID iDs

M. Tavani https://orcid.org/0000-0003-2893-1459
F. Verrecchia https://orcid.org/0000-0003-3455-5082
C. Casentini https://orcid.org/0000-0001-8100-0579
A. Ursi https://orcid.org/0000-0002-7253-9721
C. Pittori https://orcid.org/0000-0001-6661-9779
G. Piano https://orcid.org/0000-0002-9332-5319
M. Pilia https://orcid.org/0000-0001-7397-8091
G. Bernardi https://orcid.org/0000-0002-0916-7443
P. W. Cattaneo https://orcid.org/0000-0001-6877-6882
V. Fioretti https://orcid.org/0000-0002-6082-5384
F. Longo https://orcid.org/0000-0003-2501-2270
A. Morselli https://orcid.org/0000-0002-7704-9553
N. Parmiggiani https://orcid.org/0000-0002-4535-5329
S. Vercellone https://orcid.org/0000-0003-1163-1396

References

Barbiellini, G., Fedel, G., Liello, F., et al. 2002, NIMPA, 490, 146
Beloborodov, A. M. 2017, ApJL, 843, L26
Burrows, D., Hill, J., Nousek, J., et al. 2005, SSRv, 120, 165
Casentini, C., Verrecchia, F., Tavani, M., et al. 2020, ApJL, 890, L32
CHIME/FRB Collaboration, Amiri, M., Andersen, B. C., et al. 2020, arXiv:2001.10275 (C20)
CHIME/FRB Collaboration, Andersen, B. C., Bandura, K., et al. 2019, ApJL, 885, L24, (C19)
Cordes, J. M., & Chatterjee, S. 2019, ARA&A, 57, 417
Feroci, M., Costa, E., Soffitta, P., et al. 2007, NIMPA, 581, 728
Galli, M., Marisaldi, M., Fuschino, F., et al. 2013, A&A, 553, A33
Gehrels, N., Chincarini, G., Giommi, P., et al. 2004, ApJ, 611, 1005
Hankins, T. H., Kern, J. S., Weatherall, J. C., & Eilek, J. A. 2003, Natur, 422, 141
HI4PI Collaboration, Bekhti, N. B., Floer, L., et al. 2016, A&A, 594, A116
Kaspi, V. M., & Beloborodov, A. M. 2017, ARA&A, 55, 261
Labanti, C., Marisaldi, M., Fuschino, F., et al. 2009, NIMPA, 598, 470
Locatelli, N., Bernardi, G., Bianchi, G., et al. 2020, MNRAS, 494, 1229
Lorimer, D. R., Bailes, M., McLaughlin, M. A., Narkevic, D. J., & Crawford, F. 2007, Sci, 318, 777
Marcote, B., Nimmo, K., Hessels, J. W. T., et al. 2020, Natur, 577, 190, (M20)
Marisaldi, M., Labanti, C., Fuschino, F., et al. 2008, A&A, 490, 1151
Marisaldi, M., Argan, A., Ursi, A., et al. 2015, GeoRL, 42, 9481
Markwardt, C. B., Tueller, J., Skinner, G. K., et al. 2005, ApJL, 633, L77
Palmer, D. M., Barthelmy, S., Gehrels, N., et al. 2005, Natur, 434, 1107
Perotti, F., Fiorini, M., Incorvaia, S., Mattaini, E., & Sant'Ambrogio, E. 2006, NIMPA, 556, 228
Petroff, E., Hessels, J. W. T., & Lorimer, D. R. 2019, A&ARv, 27, 4
Pilia, M., Nardi, G., Bernardi, G., et al. 2020a, ATel, 13492, 1
Pilia, M., Burgay, M., Possenti, A., et al. 2020b, ApJL, submitted (arXiv:2003.12748)
Pittori, C. 2019, RLSFN, 30, 217

Prandoni, I., Murgia, M., Tarchi, A., et al. 2017, A&A, 608, A40
Tavani, M. 2019, RLSFN, 30, 38
Tavani, M., Barbiellini, G., Argan, A., et al. 2009, A&A, 502, 995
Tavani, M., Verrecchia, F., Casentini, C., et al. 2020a, ATel, 13446, 1
Tavani, M., Verrecchia, F., Casentini, C., et al. 2020b, ATel, 13462, 1
Tendulkar, S. P., Kaspi, V. M., & Patel, C. 2016, ApJ, 827, 59
Thompson, C., & Duncan, R. C. 1996, ApJ, 473, 322
Ursi, A., Tavani, M., Verrecchia, F., et al. 2019, ApJ, 871, 27